



Comparison of the Mechanical Properties and Forming Behavior of Two Texture-Weakened Mg-Sheet Alloys Produced by Twin Roll Casting

José Victoria-Hernández^{1*}, Sangbong Yi^{1*}, David Klaumünzer² and Dietmar Letzig¹

¹ Magnesium Innovation Centre, Helmholtz-Zentrum Geesthacht, Geesthacht, Germany, ² Volkswagen AG, Group Research, Materials and Manufacturing Processes, Wolfsburg, Germany

OPEN ACCESS

Edited by:

Maria Teresa Pérez,
Instituto IMDEA Materiales, Spain

Reviewed by:

Somjeet Biswas,
Indian Institute of Technology
Kharagpur, India
Xueze Jin,
Harbin Institute of Technology, China

*Correspondence:

José Victoria-Hernández
jose.victoria-hernandez@hzg.de
Sangbong Yi
sangbong.yi@hzg.de

Specialty section:

This article was submitted to
Structural Materials,
a section of the journal
Frontiers in Materials

Received: 02 July 2019

Accepted: 29 October 2019

Published: 20 November 2019

Citation:

Victoria-Hernández J, Yi S,
Klaumünzer D and Letzig D (2019)
Comparison of the Mechanical
Properties and Forming Behavior of
Two Texture-Weakened Mg-Sheet
Alloys Produced by Twin Roll Casting.
Front. Mater. 6:288.
doi: 10.3389/fmats.2019.00288

The influence of rolling and annealing on the resulting mechanical properties and forming behavior of Mg-Zn-RE and Mg-Zn-Ca alloys produced via twin roll casting is investigated. After hot rolling followed by an annealing treatment, both alloys develop a fine-grained microstructure with average grain sizes $<10\ \mu\text{m}$. A distinctive development of a texture with a pronounced split of the basal poles in the transverse direction, so called TD-split, is observed in both alloys during the annealing. Due to the fine microstructure and weak texture, which enhances the activation of basal $\langle a \rangle$ slip, both alloys show large ductility with fracture strain higher than 30%. However, due to the TD-split texture, a high asymmetry of the yield stress is observed, where the yield stress in rolling direction is significantly higher than the yield stress along 45° and the transverse direction. Both alloys show high stretch formability at room temperature with Erichsen index around 7. Despite a low planar anisotropy and high stretch formability, the Mg-Zn-RE alloy shows undesirable earing behavior, while the Mg-Zn-Ca alloy fractures during warm deep drawing. Moreover, the deep drawing operation using the as-rolled sheet of Mg-Zn-RE alloy can be successfully done. It is observed that the earing behavior can be effectively reduced by deviating from the TD-split texture. In this regard, cold rolling was explored to reduce the anisotropy of the ductile and formable alloy.

Keywords: Mg alloys, twin roll casting, rolling, texture, formability, anisotropy

INTRODUCTION

For the last two decades, wrought Mg alloys have been in constant development to improve their formability, corrosion resistance and recyclability. In 2001 the forecast of using Mg alloys was positive, especially in the automotive industry (Mordike and Ebert, 2001). So far, the relatively poor formability at low temperatures of wrought Mg alloy has still hindered its extensive use. Ways to improve the formability of Mg alloys, especially at temperatures lower than 200°C (i.e., “low temperature formability”), have been investigated and two approaches are of significant interest. The first approach is the utilization of different thermomechanical treatments to modify the crystallographic texture and, therefore, enhance the potential to activate more deformation modes during forming (Suh et al., 2015). In this regard, severe plastic deformation techniques are effective to enhance the ductility, strength of Mg alloys (Agnew et al., 2004; Biswas et al., 2010, 2013). For instance, it has been shown that alternative processing routes are effective for the

enhancement of the microstructure, i.e., grain size and texture, resulting in a decrease anisotropy of Mg alloys (Biswas and Suwas, 2012; Han et al., 2016; Suh et al., 2016). The second approach is the design of the microstructure based on changes in the chemical composition. The use of selected alloying elements has led to significant improvements in the ductility, mechanical properties and formability of wrought Mg alloys (Chino et al., 2008; Al-Samman and Li, 2011; Sandlöbes et al., 2017). Among the elements that have shown the best effects on improving the formability are the rare-earth (RE) elements. RE elements can modify important aspects on the microstructure, e.g., changes in the stacking fault energies (Sandlöbes et al., 2011, 2017), distinctive crystallographic textures (Mackenzie and Pekguleryuz, 2008; Yi et al., 2010), and precipitation which can significantly strengthen the alloys (Liu et al., 2016; Bian et al., 2017). Crystallographic textures of rolled Mg-RE alloys are normally weak and tend to develop a broad scatter of basal poles with two peaks split toward the transverse direction (TD) in (0 0 0 1) pole figure (Mackenzie and Pekguleryuz, 2008). Such textures are linked with an improvement of the low-temperature stretch formability (Chino et al., 2010a; Yi et al., 2010; Al-Samman and Li, 2011; Stutz et al., 2011a). Nevertheless, in recent years, there is a tendency to produce RE-free Mg alloys. In this regard, Ca is an effective element, which can modify the microstructure, crystallographic texture and mechanical properties in a similar way to the Mg-RE alloys (Chino et al., 2010b, 2011; Yuasa et al., 2015; Victoria-Hernandez et al., 2019). Recently, Klaumünzer et al. (2019) showed the potential of using such RE-free alloy sheets produced by twin roll casting (TRC) for the successful production of complex automotive parts for which the forming temperature can be reduced to 160°C.

Despite the good progress in improving the forming capabilities of these alloy systems showing a TD-split texture, there are only a few works dealing with the effect of this distinctive crystallographic texture on the anisotropic forming behavior. Yi et al. (2010) have shown undesirable earing during deep drawing operations of ZE10 alloy at elevated temperature. As an important forming process, deep drawing is of industrial significance and the analysis of the effect of processing parameters on the attenuation of the undesirable earing behavior is of prime importance. In this context, we conducted experiments in order to assess the forming capabilities of the Mg-Zn-RE and Mg-Zn-Ca alloys during deep drawing. Special attention has been paid to the possible reduction of the earing phenomenon by the utilization of strain-hardened blanks used directly after hot and cold rolling, i.e., without a recrystallization heat treatment. The present work gives more insights into the potential of optimizing processing parameters to enhance the forming performance of texture-weakened Mg alloys.

MATERIALS AND METHODS

TRC strips of ZEW200 (1.81Zn-0.1Nd-0.1Ce-0.05La-0.2Y in wt.%) and ZXX (0.6Zn-0.6Ca-0.1Zr in wt.%) alloys with a thickness of 5.3 mm were hot rolled (HR) to the final gauge of 1.8 mm at 400 and 370°C, respectively. The rolling schedule consists of four rolling passes with the first one applying a degree

of deformation of $\varphi = 0.25$ (true strain) and $\varphi = 0.3$ for the last three passes. Before the first rolling pass and at intermediate steps, the sheets were heated at the respective rolling temperature for 15 min. After the final rolling pass, the samples were air-cooled. A part of the ZEW200 sheets received two additional cold rolling (CR) passes at room temperature at $\varphi = 0.1$ each. In order to recrystallize the microstructure, ZEW200 samples were annealed at 350°C and ZXX samples at 370°C for 30 min.

Microstructural examination was performed by optical microscopy and electron backscatter diffraction (EBSD) on planes parallel to the normal direction (ND) and the rolling direction (RD). Samples were ground with emery paper (grit 800–2500) and polished with a water free suspension of silicon oxide (OPS 0.5 μm). The polished samples were chemically etched with a picric acid solution (150 ml of ethanol, 40 ml distilled water, 6.5 ml acetic acid and 3–4 g picric acid). The average grain size of the optical microstructures was calculated using the linear intercept method. In the case of EBSD samples, after mechanical polishing, the samples were electropolished using Struers AC2TM solution at 16 V for 70 s at -25°C . EBSD measurements were performed in a field emission gun scanning electron microscope equipped with an EDAX-TSL OIMTM system. An acceleration voltage of 15 kV and a step size of 0.3 μm were used. Energy-dispersive X-ray spectroscopy (EDS) was performed on the mechanically polished samples to reveal the type and chemical composition of the secondary phase particles near the fracture surface in a deep drawn cup.

Quantitative texture measurements were carried out using a PanalyticalTM X-ray diffractometer in reflection geometry using Cu-K α radiation. Six pole figures (0 0 0 1), (1 0 -1 0), (1 0 -1 1), (1 0 -1 2), (1 0 -1 3), and (1 1 -2 0) were measured up to a tilt angle of 70°. The orientation distribution function (ODF) was calculated using the MTEX toolbox (Hielscher and Schaeben, 2008).

Tensile samples were machined according to the standard DIN 50125-H and were tested in a universal testing machine. The tensile tests were performed along the RD, 45° and TD at room temperature, and the Lankford parameter (r_{10} -value) were determined at $\epsilon = 10\%$. Tensile tests were performed at 10^{-3} s^{-1} of constant strain rate to the fracture. This was ensured by employing a clip-on extensometer that allowed the continuous calibration of the strain rate during the experiment.

Room temperature stretch formability was evaluated by the Erichsen test using an ErichsenTM 145–30 sheet metal testing machine according to the ISO 20482. MolykoteTM was used as a lubricant. The punch diameter and test speed were 20 mm and 5 mm/min, respectively. Blanks (diameter of 60 mm) cut from the as-rolled and annealed sheets were used for the tests.

Deep drawing tests were performed in the same Erichsen machine using a punch with the diameter of 50 mm at 100, 150, and 200°C. The test speed and blank holder force were set to 20 mm/min and 5 kN. Blank diameters of 85 and 100 mm were cut from the rolled sheets for two different deep drawing ratios (DR) of 1.7 and 2.0. To minimize friction between the blank, the punch, the walls of the die and the samples were coated with boron nitride spray.

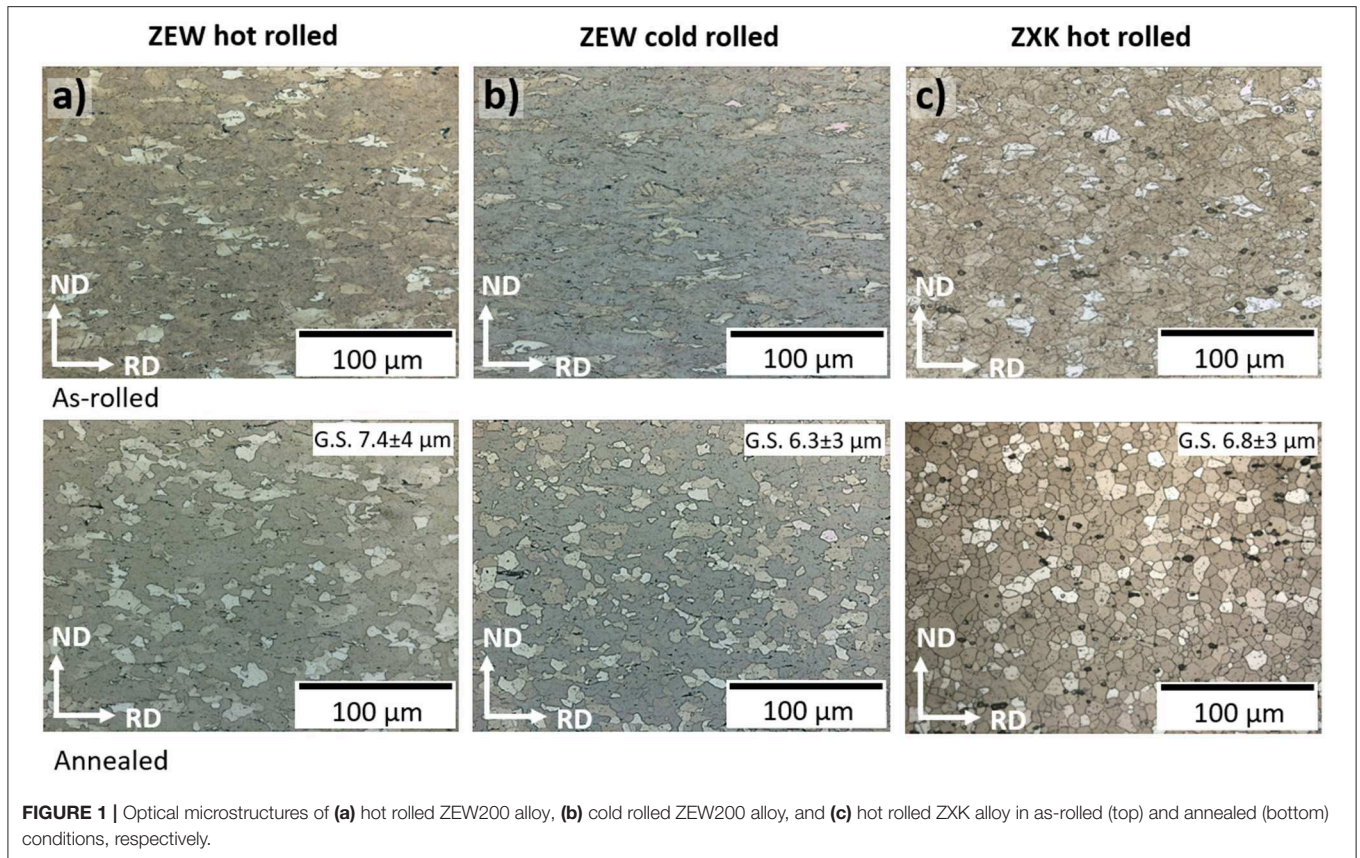


FIGURE 1 | Optical microstructures of (a) hot rolled ZEW200 alloy, (b) cold rolled ZEW200 alloy, and (c) hot rolled ZXC alloy in as-rolled (top) and annealed (bottom) conditions, respectively.

RESULTS AND DISCUSSION

Microstructure

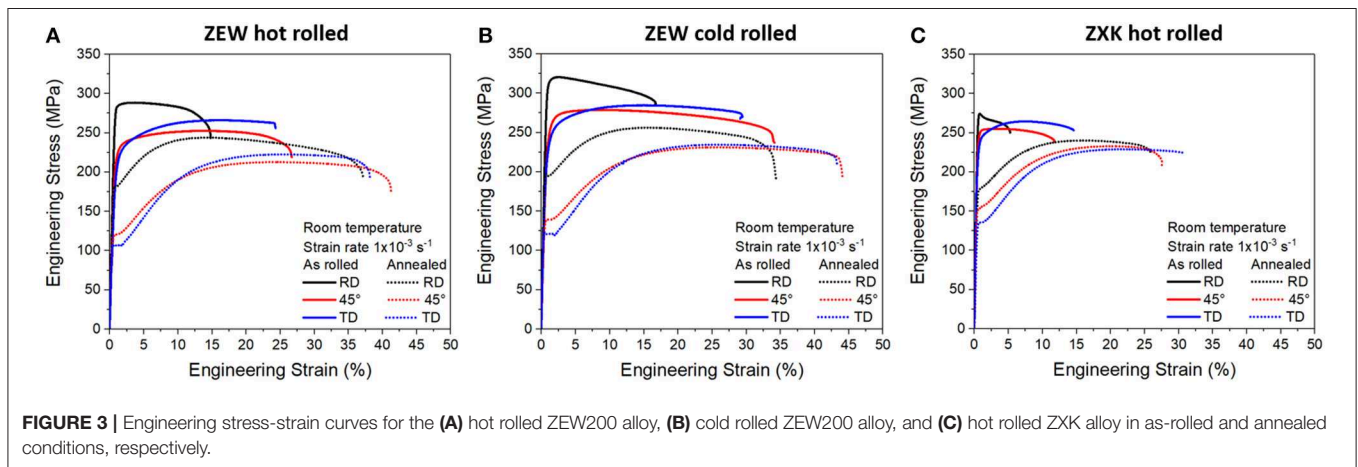
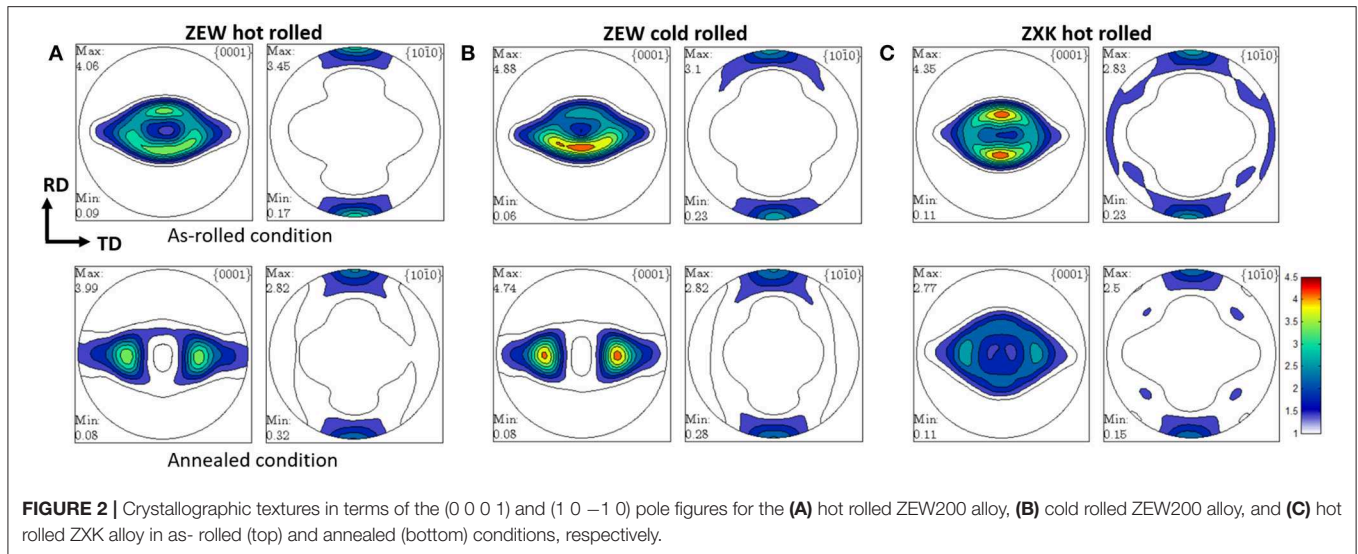
The micrographs of the rolled and annealed sheets are presented in **Figure 1**. In general, the as-rolled microstructures for the three different materials, presented in **Figures 1a–c**, show deformed grains containing twins. As expected, the microstructure of the cold-rolled ZEW200 shows a more deformed grain structure. Such a microstructure is difficult to etch chemically due to the predominance of the preferred crystallographic orientations of the grains. The ZEW200 alloy in both hot and cold rolled conditions show the presence of secondary phase particles distributed homogeneously along with the microstructure. The stinger-like precipitates contain a high amount of Zn, Ce, and Y. The rolled ZXC alloy also shows coarse precipitates. They were identified as Mg_2Ca phase. They are located along grain boundaries. Some of them are fragmented and elongated toward RD, developing stringer-like structures. The microstructure of all annealed sheets show the development of a homogeneous, fine, twin-free and recrystallized microstructure with a grain size below 10 μm.

Texture

Figure 2A depicts the texture of the hot rolled ZEW200 alloy. In the as-rolled condition, the sheet shows a relatively weak deformation texture with an intensity of 4.1 multiples of random distribution (m.r.d.). As a characteristic, two

main peaks representing (0 0 0 1) crystallographic planes tilted away from the ND toward RD and the $\langle 1\ 0\ -1\ 0 \rangle$ pole parallel to RD are observed. A broad scatter of basal poles inclined toward the TD is also evident. The annealed sheet shows a weaker texture in comparison to that of the rolled one. Moreover, the transition from the RD-split of the basal pole to a TD-split texture is observed. In this condition, the basal poles are mainly tilted by $\sim 35^\circ$ toward the TD. The texture component of $\langle 1\ 0\ -1\ 0 \rangle$ parallel to RD is retained during the annealing. Such a tendency of the texture development, i.e., weak recrystallization texture with the basal pole split into the TD, is ascribed to the activation of non-basal slip systems and retarded recrystallization kinetics in Mg-Zn-RE and Mg-Zn-Ca alloys (Kim et al., 2017; Zeng et al., 2019). Cold rolling strengthens the texture components, which were formed after hot rolling and annealing (see **Figure 2B**). However, no qualitatively different texture development is observed in comparison to the hot rolled sheet.

The deformation texture of the ZXC alloy also shows similar peaks compared to that of the ZEW200 alloy and a broad distribution of basal planes toward TD (see **Figure 2C**). This texture is slightly stronger than the hot rolled ZEW200 alloy. A weaker texture with the basal pole split toward TD is formed after annealing, while a symmetric distribution of the basal poles is observed in a ring-like fashion around the ND, at the tilting angle of $\sim 37^\circ$.



Mechanical Behavior

Figure 3 plots the engineering stress-strain curves of samples in the as-rolled and annealed states. The corresponding tensile properties are listed in **Table 1**. The hot rolled ZEW200 alloy in the as-rolled condition shows an overall high strength level in all planar sheet directions. However, anisotropic behavior is observed with the strength values in the RD being the highest. Interestingly, the ductility is relatively high for a strain-hardened Mg alloy with elongations higher than 20% along both the 45° and TD, and 19% in RD (see **Figure 3A**). After annealing, the sheet shows an increase in ductility along all directions with the fracture strain higher than 35%. The annealed sheets show a distinct yield phenomenon. Various mechanisms of the occurrence of yield phenomenon in Mg alloys have been reported, e.g., twinning (Barnett et al., 2012), activity of non-basal slip (Koike et al., 2003) or dislocation interaction with solute atoms (Zhang et al., 2010). A high planar anisotropy is observed also in the annealed sheets. The sample tested parallel to the RD shows high strength and rapid work hardening in comparison to 45° and TD samples. The cold rolled samples in

the as-rolled state show even higher strength, exceeding 300 MPa in the RD. Surprisingly, a drop in the ductility is not observed when contrasted to the hot rolled samples. The material remains ductile in all directions as shown in **Figure 3B**. The annealed samples after the cold rolling show a high planar anisotropy, while an increase in ductility is observed (larger than 40% along 45° and TD). The improvement of mechanical properties can be mainly attributed to the grain refinement as displayed in **Figure 1b**, since the texture is rather similar to the hot rolled sheets.

Recently Shi et al. (2019) have reported the possibility to reduce the planar anisotropy of Mg-Zn-Y-Zr alloy sheets by applying the final rolling pass with a high reduction degree. It was shown that the anisotropic effect of the TD-split texture was attenuated by increasing the deformation and controlling the post-annealing. In the present study, however, the reduction in the planar anisotropy determined by tensile tests was not observed even after cold rolling.

In contrast to the behavior of the ZEW200 alloy, the ZKX alloy shows a more moderate planar anisotropy, where the

TABLE 1 | Tensile properties at room temperature of as-rolled and annealed samples tested along RD, 45° to RD and TD (YS, tensile 0.2% yield stress; UTS, ultimate tensile stress, ϵ_u , uniform elongation; ϵ_f , elongation to fracture, r_{10} Lankford parameter).

		YS (MPa)	UTS (MPa)	ϵ_u (%)	ϵ_f (%)	r_{10} -value	\bar{r}	Δr
ZEW HR AR	RD	270 ± 2	288 ± 2	3	19	1.1 ± 0.1*	0.88	0.15
	45°	197 ± 3	250 ± 2	13	26	0.8 ± 0.1		
	TD	190 ± 5	266 ± 2	16	20	0.8 ± 0.1		
ZEW HR Annealed	RD	181 ± 4	244 ± 4	14	33	1.2 ± 0.1	0.85	−0.10
	45°	118 ± 4	215 ± 3	22	40	0.9 ± 0.1		
	TD	106 ± 3	221 ± 4	24	35	0.4 ± 0.1		
ZEW CR AR	RD	298 ± 2	320 ± 4	2	16	0.6 ± 0.1*	0.88	−0.45
	45°	220 ± 3	282 ± 2	8	33	1.1 ± 0.1*		
	TD	205 ± 3	286 ± 2	14	27	0.7 ± 0.1		
ZEW CR Annealed	RD	197 ± 3	257 ± 2	15	33	0.7 ± 0.1	0.80	−0.40
	45°	134 ± 3	231 ± 2	25	43	1.0 ± 0.1		
	TD	121 ± 2	232 ± 3	26	42	0.5 ± 0.1		
Z XK AR	RD	255 ± 2	276 ± 2	1	8	1.1 ± 0.1*	1.10	−0.20
	45°	217 ± 3	255 ± 2	5	19	1.2 ± 0.1*		
	TD	200 ± 2	265 ± 2	12	23	0.9 ± 0.1		
Z XK HR Annealed	RD	174 ± 3	239 ± 3	16	25	0.9 ± 0.1	0.98	−0.25
	45°	152 ± 3	232 ± 2	19	27	1.1 ± 0.1		
	TD	135 ± 2	226 ± 2	21	31	0.8 ± 0.1		

* r -value measured at $\epsilon_u < 10\%$.

differences in yield stress, UTS and fracture strain are generally smaller compared to the ZEW alloy (see **Figure 3C**). The reduced anisotropy at the annealed state is to be related to the texture of the Z XK alloy and the relatively uniform scatter of basal planes, which develop a ring of basal poles around the ND.

The r -values strongly vary upon heat treatments. Especially for ZEW200 alloy along the TD, the r -value decreases after annealing, which can be related to the development of a more pronounced TD-split in the texture (see **Figures 2A,B**). The average \bar{r} -values and planar anisotropy Δr were calculated at each condition, according to the following relationships:

$$\bar{r} = \frac{(r_{RD} + r_{TD} + 2r_{45})}{4}$$

$$\Delta r = \frac{(r_{RD} + r_{TD} - 2r_{45})}{2}$$

where r_{RD} , r_{45} , r_{TD} are the r -values determined in RD, 45° to RD and TD, respectively. The calculated values are listed in **Table 1**. It is observed that the \bar{r} -values of the ZEW200, even after the cold rolling, are lower than those of the Z XK alloy. These results indicate that the material flow in the thickness direction is easier in the ZEW200, while the Z XK sheets with the \bar{r} -values close to 1 show a comparable material flow in the thickness and width directions. The uniform distribution of basal planes with a ring-fashioned texture in the Z XK sheet leads to a reduction of the anisotropy, and less pronounced earing is expected during deep drawing. Based on the magnitude of planar anisotropy (Δr), e.g., $\Delta r = -0.10$ and -0.25 in the annealed ZEW200 HR and Z XK HR sheets, respectively, the Z XK alloy would have a higher propensity of earing. However, the r -values of the ZEW200 sheet show a higher variation along the

sheet planar direction, comparing to those measured from the Z XK sheet. Such inconsistency results from the fact that the planar anisotropy in Mg alloys is different to that in the cubic structured materials.

For example, Yi et al. (2010) reported that the earing is observed at 60° to the RD of a deep drawn cup of ZE10 sheet, such that the asymmetric deformation behavior of Mg alloy sheets would not be completely expressed by the r -values measured at the RD, TD, and 45° to the RD. It should be noted that the r -value analysis in the present study corresponds to an approximate estimate, as the r -values of some samples were determined at rather low uniform strain, e.g., samples marked with asterisk.

Formability Erichsen Tests

To evaluate the stretch formability at room temperature, Erichsen tests were performed using blanks in as-rolled and annealed conditions. Samples after Erichsen tests are shown in **Figure 4**. Even in the as-rolled condition, the hot rolled ZEW200 alloy showed a relatively high Erichsen index (IE) of 5.1. The IE of the ZEW200 alloy increases in the annealed condition to 7.4 (see **Figure 4a**). Upon cold rolling, the stretch formability for the as-cold rolled ZEW200 alloy decreases to the IE of 3.1, which increases significantly after annealing to the IE of 8.4. This is one of the highest values recorded for conventionally rolled Mg alloys and it shows the potential to improve the sheet formability by means of altering the processing route, such as cold rolling.

For the hot rolled Z XK alloy the average IE of 3.7 and 6.2 were obtained at the as-rolled and annealed conditions, respectively. Despite the fact that the Z XK alloy showed the lowest texture intensity and a ring scatter of basal poles around the ND in

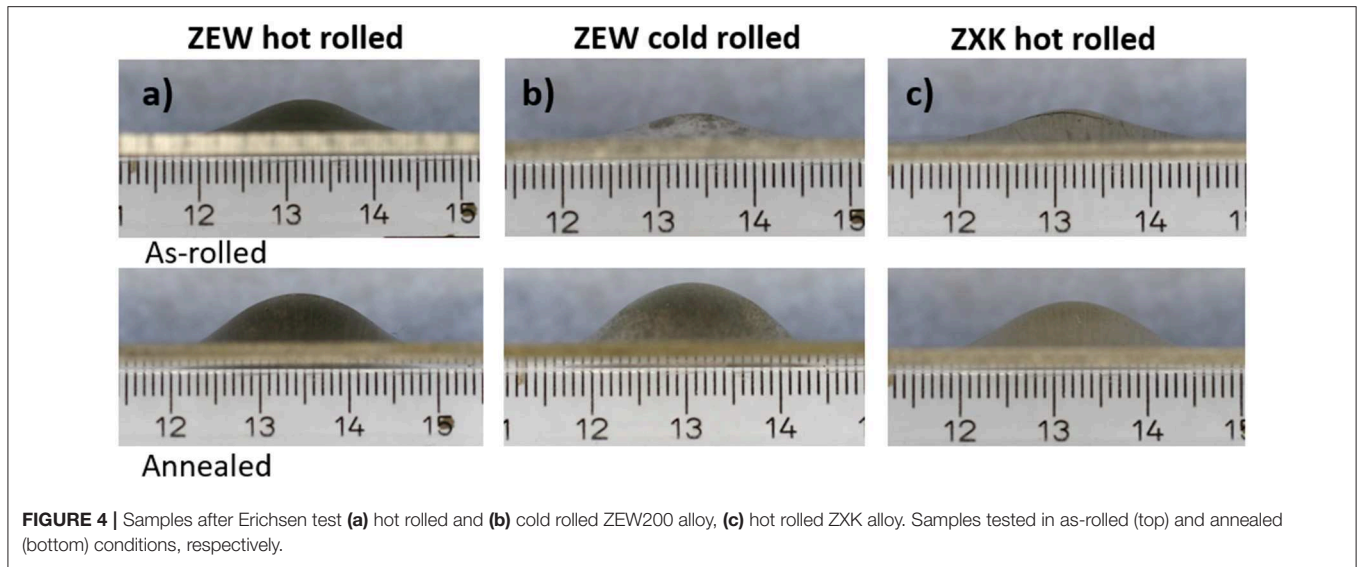


FIGURE 4 | Samples after Erichsen test (a) hot rolled and (b) cold rolled ZEW200 alloy, (c) hot rolled ZXC alloy. Samples tested in as-rolled (top) and annealed (bottom) conditions, respectively.

the annealed condition, the recorded IE is lower than those of annealed ZEW200 alloy. Other microstructural factors, such as the presence of Mg_2Ca particles and Mg oxides, could be related to the crack initiation or ease propagation during stretch forming. Nevertheless, the present results confirm that the stretch formability at room temperature is enhanced with the formation of the characteristic TD-split texture in the Mg-Zn-RE and Mg-Zn-Ca alloys.

Deep Drawing at Warm Temperatures

The deep drawability of the hot rolled and annealed ZEW200 and ZXC alloys was assessed at 100, 150, and 200°C and a DR of 1.7. Representative samples deformed at these conditions are displayed in **Figure 5**. In the case of the ZEW200 alloy, deep drawing can be successfully conducted at 100°C (see **Figure 5a**). There is, however, the development of fractures, which occurred at the top part of the wall of the sample. Yi et al. (2010) have attributed the development of these kinds of defects to the non-optimized process parameters, such as blank holder force or clearance. In addition, the temperature gradient in the sample during the test could affect the sample thickening toward the top area of the cup wall, leading to increased friction between the sample and the die (Ghosh et al., 2014). Yet, the present result supports that the deep drawing is feasible at 100°C, if the parameters are properly adjusted. By increasing the temperature, successfully drawn cups are obtained. There is the development of slight earing on both cups, which seem to be similar in number (4), height and position ($\sim 63^\circ$ to RD). This undesirable phenomenon seems to be independent on the forming temperature.

Despite the good stretch formability shown at room temperature by the ZXC alloy, the deep drawability is rather poor. Samples deformed at 100°C develop catastrophic failures at the shoulder of the cup, which propagates to the flange of the cup. This behavior is also observed for samples deformed at 150°C. In contrast, samples deformed at 200°C showed slightly better

behavior in comparison to the previous two cases. Yet, fractures at the top of the wall are observed (see **Figure 5b**). This result is interesting, considering that both alloys have a similar initial microstructure, i.e., grain size and, in principle, crystallographic texture. It is found, however, that coarse precipitates of Mg_2Ca and oxides seem to have relationship with the brittle behavior at warm temperatures of the ZXC alloy. **Figure 6a** depicts an optical micrograph of a polished sample; it shows a fracture front of a sample drawn at 150°C. The approximate position of the analysis is marked with the white-filled arrow in **Figure 5**. The accumulation of particles is found at the crack front, marked as dotted square in **Figure 6a**. An SEM-image at this area shows the fragmentation of such particles (see **Figure 6b**). An element mapping using EDX showed that those particles mainly consist of Ca and O (see **Figures 6c,d**). The presence of those elements correlate well with high amount of hard and brittle Mg_2Ca Laves phase, in addition to the presence of MgO and/or CaO. The fragmentation and respective void formation around these particles are, therefore, related to the ease nucleation and propagation of crack during the warm deep drawing of the ZXC alloy. It was reported in Jahedi et al. (2018) that the shearing of eutectic particles and concomitant void formation lead to catastrophic failure of WE43 alloy. In such work it is discussed the more influential effect of void formation (due to particle shearing) than the texture effect during deformation. The fragmentation of particles, e.g., Mg_2Ca and oxides, and resulting void formation can be also correlated with the lower IE of ZXC alloy in the present study.

In order to gain more insight into the deformation behavior of the examined alloys, the microstructure at the wall was analyzed by means of EBSD. **Figure 7** exhibits the EBSD orientation maps of samples deformed at 100 and 200°C of the ZEW200 and ZXC alloys. The approximate position of the measurement is marked by the dotted squares in **Figure 5**. The ZEW200 sample deformed at 100°C presents a highly deformed microstructure with the presence of twins (**Figure 7A**). The

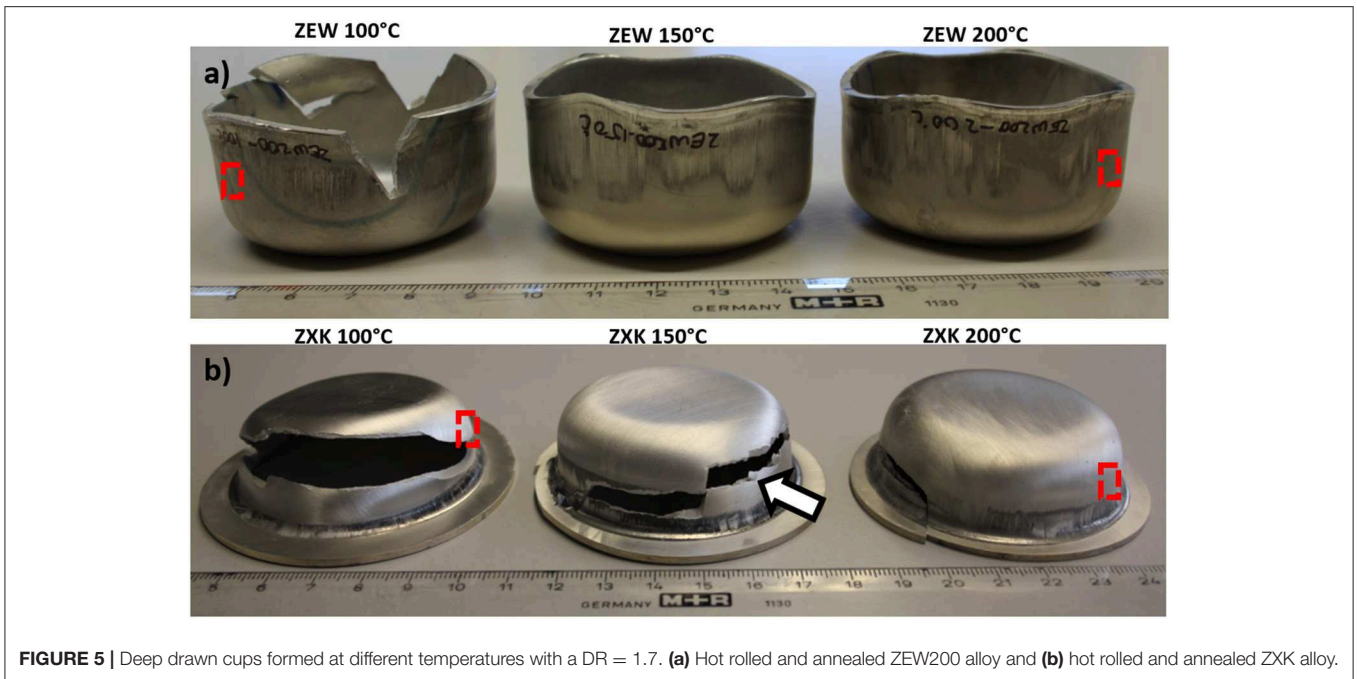


FIGURE 5 | Deep drawn cups formed at different temperatures with a DR = 1.7. **(a)** Hot rolled and annealed ZEW200 alloy and **(b)** hot rolled and annealed ZKX alloy.

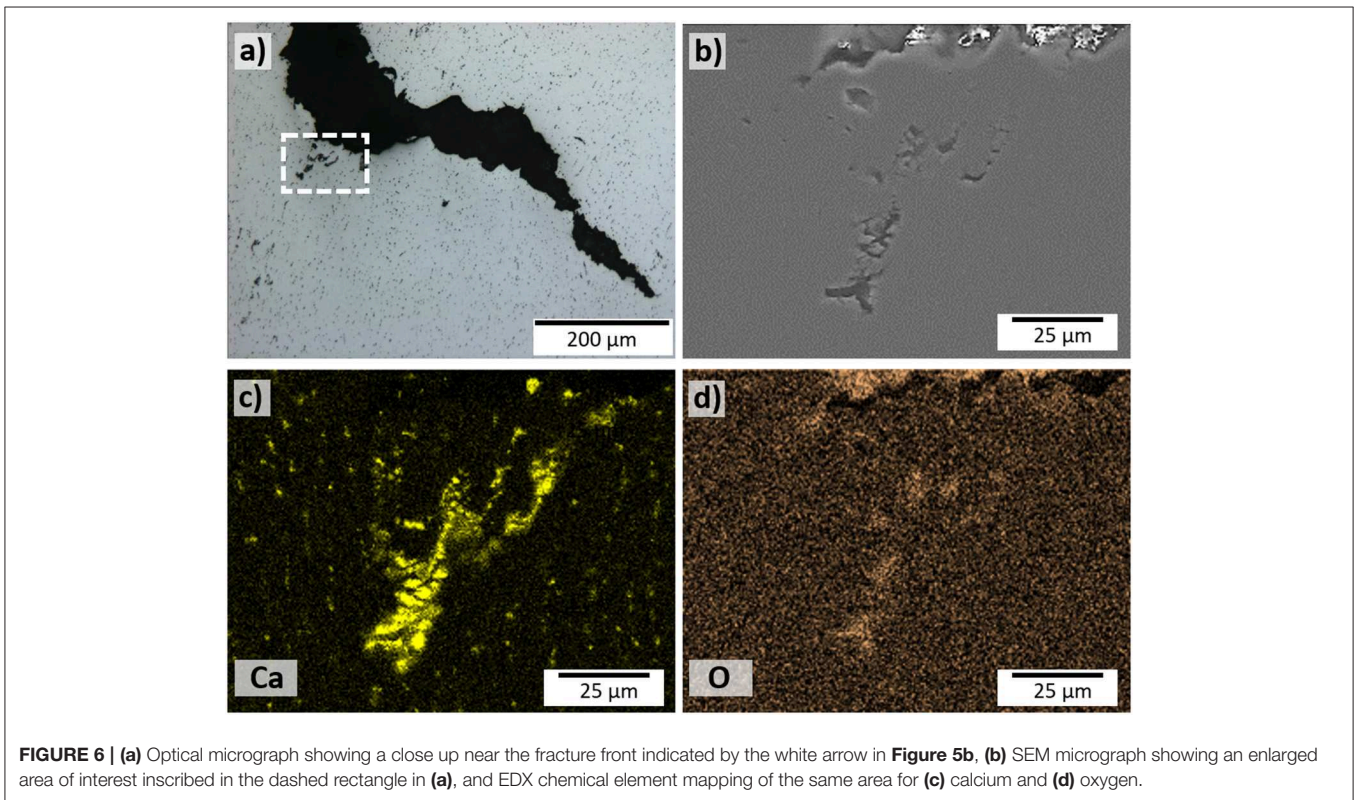
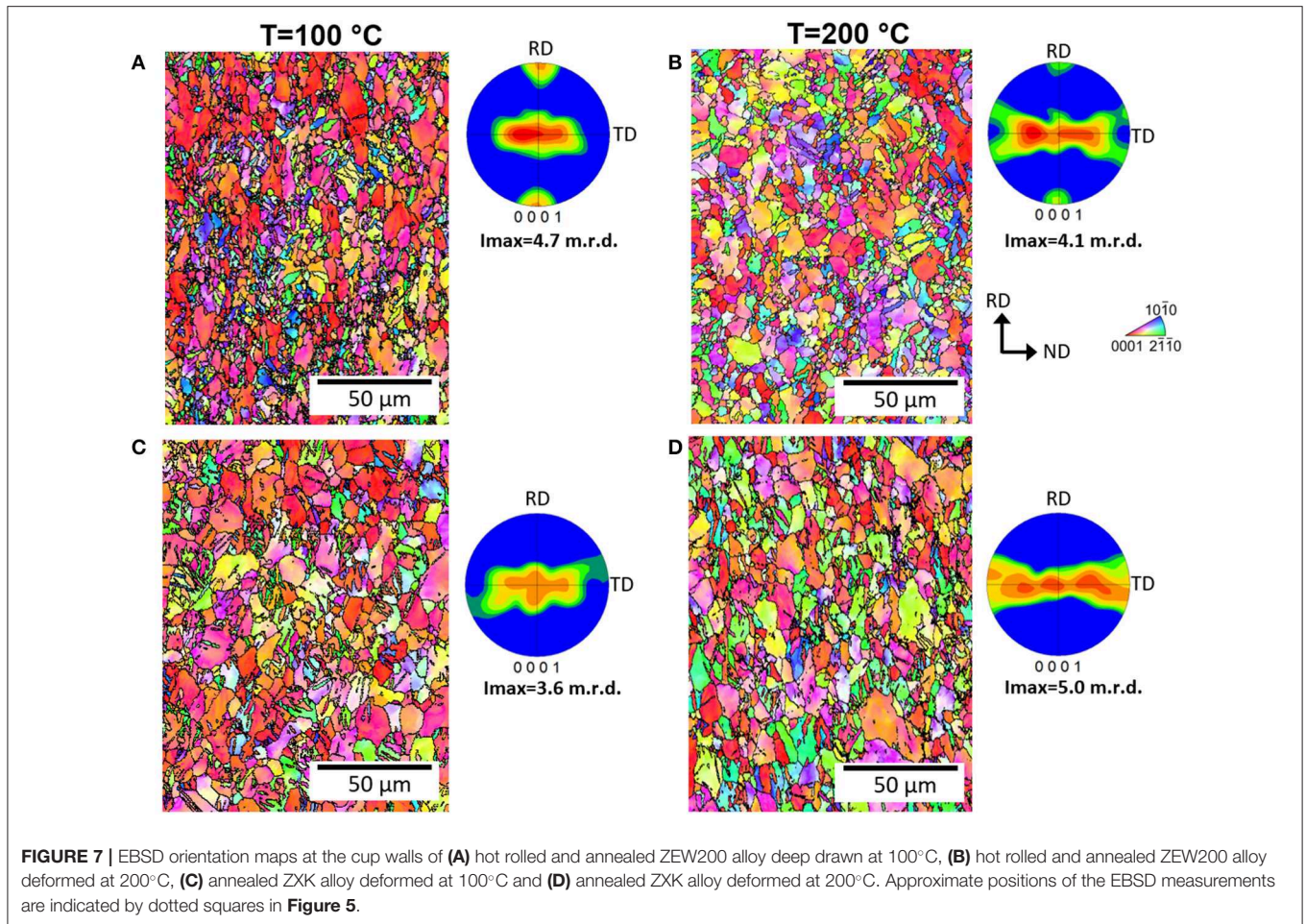


FIGURE 6 | **(a)** Optical micrograph showing a close up near the fracture front indicated by the white arrow in **Figure 5b**, **(b)** SEM micrograph showing an enlarged area of interest inscribed in the dashed rectangle in **(a)**, and EDX chemical element mapping of the same area for **(c)** calcium and **(d)** oxygen.

identified twinning mode mainly corresponds to $\{1\ 0\ -1\ 2\}$ extension twins covering an area fraction of around 7.4%. Other detected twinning modes, such as $\{1\ 0\ -1\ 1\}$ contraction twins and $\{1\ 0\ -1\ 1\}$ - $\{1\ 0\ -1\ 2\}$ secondary twins are seldom detected and the area fraction covered by these two systems is $<1\%$. A strengthening of the texture toward basal type texture is also

observed. Tests conducted at 200°C show similar microstructures (**Figure 7B**). The extension twin fraction is also high, covering about 6.5% of the microstructure. In this case, there is the tendency to strengthen the texture but the broad scatter of basal planes toward TD is still high. Yi et al. (2010) explained this phenomenon by the profuse activation of prismatic $\langle a \rangle$ slip.



Despite the significantly lower deformation degree attained by the ZXC samples, a similar tendency in microstructure and texture development is observed. That is, $\{1\ 0\ -1\ 2\}$ extension twins are profusely activated, and a basal type texture develops at 100°C, while the broad scatter of basal planes toward TD is formed at 200°C (see **Figures 7C,D**, respectively). The present result once again shows the similarities of the involved deformation mechanisms in both alloys. Therefore, it might be feasible to improve the formability of the ZXC alloy by optimization of the alloy composition and processing parameters to control the amount, size and distribution of the brittle Mg_2Ca particles.

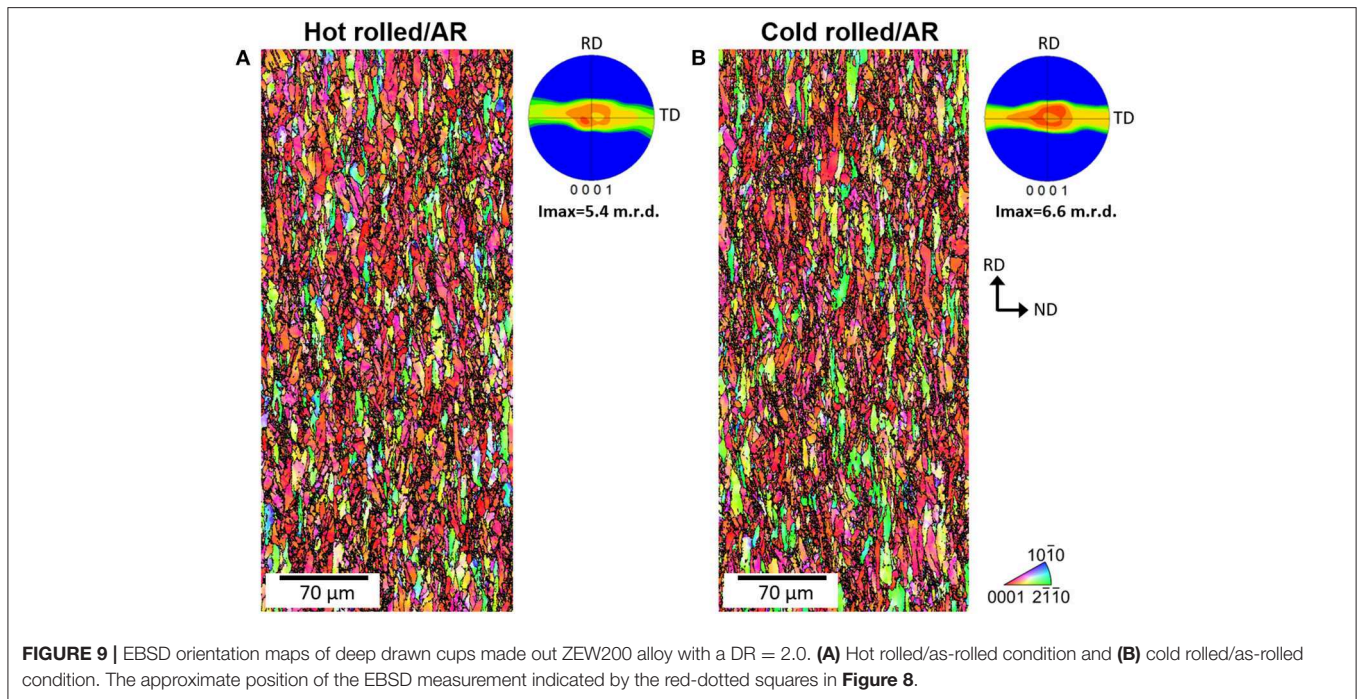
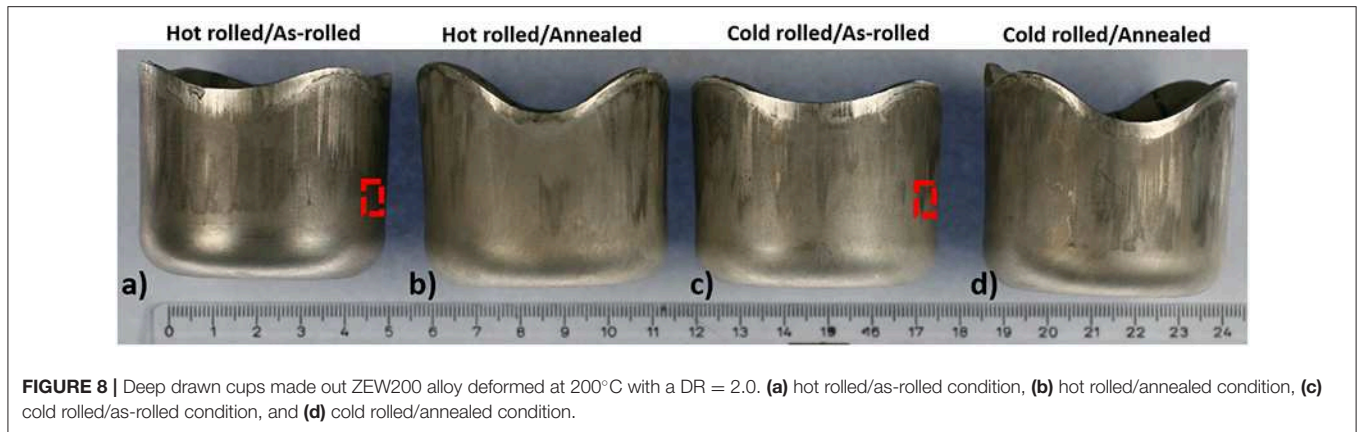
The earing behavior of the cold rolled ZEW200 alloy was investigated by using the blanks of 100 mm in diameter at 200°C ($\text{DR} = 2$) in the as-rolled and annealed conditions. Representative drawn cups are shown in **Figure 8**. Cups could be drawn fully using blanks even in the as-rolled condition. Moreover, the earing behavior is reduced by the use of the blanks in the as-rolled conditions, **Figures 8a,c**. To describe the degree of earing, the average percentage of earing height (Z) was calculated according to the following equation. This equation, which is capable of describing earing even if local asymmetry occurs, is used based on the position of the ears which are not located at

0, 45, or 90° as it normally occurs in metals with cubic structure (Yi et al., 2010).

$$Z = \left[\left[\sum_i^n \left(\frac{h_{i_{\max}} - h_{i_{\min}}}{0.5(h_{i_{\max}} + h_{i_{\min}})} \right) \right] / n \right] \times 100 (\%)$$

where n is the number of ears in the drawn cup, and h is the height at the peak and valleys of each ear observed in the drawn cup. The earing degrees (Z) of the hot rolled sheet is 9.7% in the as-rolled condition and 15.9% after annealing. A similar tendency is observed in the cold rolled sheet, where Z for the as-rolled sheet is 9.9% and increases to 16.8% after annealing. This means that cold rolling can strengthen the material (as observed in **Figure 3**), and increases the anisotropic behavior after annealing, e.g., increase in the earing behavior.

Analogous to the analysis presented in **Figure 7**, the microstructures at the wall of the successfully drawn cups deformed at 200°C using hot/cold as-rolled sheets of the ZEW200 alloy are presented in **Figure 9**. The approximate positions of the EBSD measurements are marked with the red dashed rectangles in **Figure 8**. A highly deformed microstructure is found in both cases, where most of the grains are elongated parallel to the drawing direction. The formation of shear bands



around the deformed grains is also evident. It is to note that the amount of recrystallized grains is maintained to a minimum despite the use of a strain hardened materials. These results indicate that the deformation is mainly accommodated by dislocation slip (in this case is hard to identify twin boundaries in the OI maps) and dynamic recovery, rather than dynamic recrystallization. This is one of the main differences compared to the deep drawing behavior of conventional AZ31 alloy, where dynamic recrystallization is an important softening mechanism that enhances the drawability at temperatures around 200°C (Yi et al., 2010; Stutz et al., 2011b). As observed in the local texture of these two as-rolled ZEW200 deformed samples, the texture is more strengthened in the as-cold rolled sheet. This could be one of the reasons for the slightly higher anisotropy as calculated by the Z factor as discussed above.

SUMMARY

A comparative study of the mechanical behavior, room temperature stretch formability and warm drawability of Mg-Zn-RE and Mg-Zn-Ca alloys with TD-split texture were carried out. Main conclusions are drawn below:

1. Upon hot rolling and subsequent annealing, both ZEW200 and ZXX alloys develop fine-grained microstructures and the so-called TD-split texture is found. By performing cold rolling in the ZEW200 the microstructure can be refined further and a stronger deformation texture than the counterpart hot rolled sheet is observed.

2. The hot/cold rolled ZEW200 alloys show high strength and high ductility. The annealing of the cold rolled sheets improves the ductility and strength in the ZEW200 alloy, whereas a high

yield stress asymmetry is observed. The ZXK alloy showed a moderate anisotropy due to its ring-fashioned texture.

3. The hot/cold rolled ZEW200 alloys show a high stretch formability, even in the as-rolled condition. The Erichsen index of 8.4 was attained for the annealed ZEW200 sheet after cold rolling. The ZXK alloy also showed good stretch formability, but IE values are lower than those of ZEW200 alloy.

4. The ZXK alloy shows a poor warm drawability. This is related to the fragmentation of hard and brittle Mg₂Ca and oxide particles with the concomitant void formation and crack propagation. On the other hand, the ZEW200 alloy shows an excellent deep drawability, even though a high anisotropy is observed. The earing behavior of this alloy was attenuated by using blanks without annealing. Analysis of the deformed microstructure indicated a profuse activity of dislocation slip during the deep drawing of the as-rolled sheets. As a softening mechanism, dynamic recovery seems to be important as the occurrence of dynamic recrystallization is not observed. It is concluded that the suppression of the TD-split texture can be an effective way to reduce anisotropic behavior of these ductile Mg alloys.

REFERENCES

- Agnew, S. R., Horton, J. A., Lillo, T. M., and Brown, D. W. (2004). Enhanced ductility in strongly textured magnesium produced by equal channel angular pressing. *Scripta Mater.* 50, 377–381. doi: 10.1016/j.scriptamat.2003.10.006
- Al-Samman, T., and Li, X. (2011). Sheet texture modification in magnesium based alloys by selective rare earth alloying. *Mater. Sci. Eng. A* 528, 3809–3022. doi: 10.1016/j.msea.2011.01.080
- Barnett, M., Nave, M. D., and Ghaderi, A. (2012). Yield point elongation due to twinning in a magnesium alloy. *Acta Mater.* 60, 1433–1443. doi: 10.1016/j.actamat.2011.11.022
- Bian, M. Z., Sasaki, T. T., Suh, B. C., Nakata, T., Kamado, S., and Hono, K. (2017). A heat treatable Mg-Al-Ca-Mn-Zn sheet alloy with good room temperature formability. *Scripta Mater.* 138, 151–155. doi: 10.1016/j.scriptamat.2017.05.034
- Biswas, S., Beausir, B., Toth, L., and Suwas, S. (2013). Evolution of texture and microstructure during hot torsion of a magnesium alloy. *Acta Mater.* 61, 5263–5277. doi: 10.1016/j.actamat.2013.05.018
- Biswas, S., Dhinwal, S. S., and Suwas, S. (2010). Room temperature equal channel angular extrusion of pure magnesium. *Acta Mater.* 58, 3247–3261. doi: 10.1016/j.actamat.2010.01.051
- Biswas, S., and Suwas, S. (2012). Evolution of sub-micron grain size and weak texture in magnesium alloy Mg-3Al-0.4Mn by a modified multi-axial forging process. *Scripta Mater.* 66, 89–92. doi: 10.1016/j.scriptamat.2011.10.008
- Chino, Y., Huang, X., Suzuki, K., and Mabuchi, M. (2010b). Enhancement of stretch formability at room temperature by addition of Ca in Mg-Zn alloy. *Mater. Trans.* 51, 818–821. doi: 10.2320/matertrans.M2009385
- Chino, Y., Huang, X., Suzuki, K., Sassa, K., and Mabuchi, M. (2010a). Influence of Zn concentration on stretch formability at room temperature of Mg-Zn-Ce alloy. *Mater. Sci. Eng. A* 528, 566–572. doi: 10.1016/j.msea.2010.09.081
- Chino, Y., Kado, M., and Mabuchi, M. (2008). Enhancement of tensile ductility and stretch formability of magnesium by addition of 0.2 wt% (0.035 at%) Ce. *Mater. Sci. Eng. A* 494, 343–349. doi: 10.1016/j.msea.2008.04.059
- Chino, Y., Ueda, T., Otomatsu, Y., Sassa, K., Huang, X., Suzuki, K., et al. (2011). Effects of Ca on tensile properties and stretch formability at room temperature in Mg-Zn and Mg-Al alloys. *Mater. Trans.* 52, 1477–1482. doi: 10.2320/matertrans.M2011048
- Ghosh, M., Miroux, A., Werkhoven, R. J., Bolt, P. J., and Kestens, L. A. I. (2014). Warm deep drawing and post drawing analysis of two Al-Mg-Si alloys. *J. Mater. Proc. Tech.* 214, 756–766. doi: 10.1016/j.jmatprotec.2013.10.020
- Han, T., Huang, G., Wang, Y., Wang, G., Zhao, Y., and Pan, F. (2016). Enhanced mechanical properties of AZ31 magnesium alloy sheets by continuous bending process after V-bending. *Prog. Nat. Sci. Mater.* 26, 97–102. doi: 10.1016/j.pnsc.2016.01.005
- Hielscher, R., and Schaeben, H. (2008). A novel pole figure inversion method: specification of the MTEX algorithm. *J. Appl. Crystallogr.* 41, 1024–1037. doi: 10.1107/S0021889808030112
- Jahedi, M., McWilliams, B. A., and Knezevic, M. (2018). Deformation and fracture mechanisms in WE43 magnesium-rare earth alloy fabricated by direct-chill casting and rolling. *Mater. Sci. Eng. A* 726, 194–207. doi: 10.1016/j.msea.2018.04.090
- Kim, Y. M., Mendis, C., Sasaki, T., Letzig, D., Pyczak, F., Hono, K., et al. (2017). Static recrystallization behavior of cold rolled Mg-Zn-Y alloy and role of solute segregation in microstructure evolution. *Scripta Mater.* 136, 41–45. doi: 10.1016/j.scriptamat.2017.04.001
- Klaumünzer, D., Victoria-Hernandez, J., Yi, S., Letzig, D., Kim, S. H., Kim J. J., et al. (2019) “Magnesium process and alloy development for applications in the automotive industry,” in *Magnesium Technology, The Minerals, Metals and Materials Series*, San Antonio, Texas, USA, eds V. Joshi, J. Jordon, D. Orlov, and N. Neelameggham (Cham: Springer), 15–20. doi: 10.1007/978-3-030-05789-3_3
- Koike, J., Kobayashi, T., Mukai, T., Watanabe, H., Suzuki, M., Maruyama, K., et al. (2003). The activity of non-basal slip systems and dynamic recovery at room temperature in fine-grained AZ31B magnesium alloys. *Acta Mater.* 51, 2055–2065. doi: 10.1016/S1359-6454(03)00005-3
- Liu, L., Chen, X., Pan, F., Gao, S., and Zhao, C. (2016). A new high strength Mg-Zn-Ce-Y-Zr magnesium alloy. *J. Alloys Compd.* 688, 537–541. doi: 10.1016/j.jallcom.2016.07.144
- Mackenzie, L. W. F., and Pekguleryuz, M. O. (2008). The recrystallization and texture of magnesium-zinc-cerium alloys. *Scripta Mater.* 59, 665–668. doi: 10.1016/j.scriptamat.2008.05.021
- Mordike, B. L., and Ebert, T. (2001). Magnesium properties-applications-potential. *Mater. Sci. Eng. A* 302, 37–45. doi: 10.1016/S0921-5093(00)01351-4

DATA AVAILABILITY STATEMENT

The datasets of this investigation cannot be shared at this moment, since they are part of an on-going investigation.

AUTHOR CONTRIBUTIONS

The study was conceived and designed by JV-H and SY. All authors took part in the discussion about the results. The manuscript was prepared by JV-H, and reviewed and edited by SY, DK, and DL. All authors approved the manuscript.

FUNDING

This work was partly financed by Volkswagen AG (Germany) and POSCO (South Korea).

ACKNOWLEDGMENTS

The technical assistance of Alexander Reichert, Guadalupe Cano-Castillo, and Deik Petersen at Helmholtz-Zentrum Geesthacht is gratefully acknowledged.

- Sandlöbes, S., Friák, M., Korte-Kerzel, S., Pei, Z., Neugebauer, J., and Raabe, D. (2017). A rare earth free magnesium alloy with improve intrinsic ductility. *Sci. Rep.* 7, 1–8. doi: 10.1038/s41598-017-10384-0
- Sandlöbes, S., Zaefferer, S., Schestakow, I., Yi, S., and Gonzalez-Martinez, R. (2011). On the role of non-basal deformation mechanisms for the ductility of Mg and Mg-Y alloys. *Acta Mater.* 59, 429–439. doi: 10.1016/j.actamat.2010.08.031
- Shi, B. Q., Xiao, Y. H., Shang, X. L., Cheng, Y. Q., Yan, H., Dong, Y., et al. (2019). Achieving ultra-low planar anisotropy and high stretch formability in a Mg-1.1Zn-0.7Y-0.56Zr sheet by texture tailoring via final-pass heavy reduction. *Mater. Sci. Eng. A* 746, 115–126. doi: 10.1016/j.msea.2018.12.116
- Stutz, L., Bohlen, J., Letzig, D., and Kainer, K. U. (2011a). “Formability of magnesium sheet ZE10 and AZ31 with respect to initial texture,” in *Magnesium Technology*, The Minerals, Metals and Materials Society, San Diego, California, USA, eds W. H. Sillekens, S. R. Agnew, N. R. Neelameggham, and S. N. Mathaudhu (J. Wiley and Sons, Inc.), 373–378. doi: 10.1002/9781118062029.ch6
- Stutz, L., Quade, J., Dahms, M., Letzig, D., and Kainer, K. U. (2011b). Achievements in deep drawing of AZ31 magnesium alloy sheets. *Mater. Sci. Forum.* 690, 302–305. doi: 10.4028/www.scientific.net/MSF.690.302
- Suh, J., Victoria-Hernandez, J., Letzig, D., Golle, R., Yi, S., Bohlen, J., et al. (2015). Improvement in cold formability of AZ31 magnesium alloy sheets processed by equal channel angular pressing. *J Mater. Proc. Tech.* 217, 286–293. doi: 10.1016/j.jmatprotec.2014.11.029
- Suh, J., Victoria-Hernandez, J., Letzig, D., and Golle, Volk W. (2016). Effect of processing route on texture and cold formability of AZ31 Mg alloy sheets processed by ECAP. *Mater. Sci. Eng. A* 669, 159–170. doi: 10.1016/j.msea.2016.05.027
- Victoria-Hernandez, J., Yi, S., Klaumünzer, D., and Letzig, D. (2019). Recrystallization behavior and its relationship with deformation mechanisms of a hot rolled Mg-Zn-Ca-Zr alloy. *Mater. Sci. Eng. A* 761:138054. doi: 10.1016/j.msea.2019.138054
- Yi, S., Bohlen, J., Heinemann, F., and Letzig, D. (2010). Mechanical anisotropy and deep drawing behavior of AZ31 and ZE10 magnesium alloy sheets. *Acta Mater.* 58, 592–605. doi: 10.1016/j.actamat.2009.09.038
- Yuasa, M., Miyazawa, N., Hayashi, M., Mabuchi, M., and Chino, Y. (2015). Effects of group II elements on the cold stretch formability of Mg-Zn alloys. *Acta Mater.* 83, 294–303. doi: 10.1016/j.actamat.2014.10.005
- Zeng, X., Minárik, P., Dobron, P., Letzig, D., Kainer, K. U., and Yi, S. (2019). Role of deformation mechanisms and grain growth in microstructure evolution during recrystallization of Mg-Nd alloys. *Scripta Mater.* 166, 53–57. doi: 10.1016/j.scriptamat.2019.02.045
- Zhang, J., Zhang, X., Li, W., Pan, F., and Guo, Z. (2010). Partition of Er among the constituent phases and the yield phenomenon in a semi-continuously cast Mg-Zn-Zr alloy. *Scripta Mater.* 63, 367–370. doi: 10.1016/j.scriptamat.2010.04.015

Conflict of Interest: The authors declare that the research was conducted in the absence of any commercial or financial relationships that could be construed as a potential conflict of interest.

Copyright © 2019 Victoria-Hernández, Yi, Klaumünzer and Letzig. This is an open-access article distributed under the terms of the Creative Commons Attribution License (CC BY). The use, distribution or reproduction in other forums is permitted, provided the original author(s) and the copyright owner(s) are credited and that the original publication in this journal is cited, in accordance with accepted academic practice. No use, distribution or reproduction is permitted which does not comply with these terms.